

See discussions, stats, and author profiles for this publication at: <https://www.researchgate.net/publication/40828885>

Isotropic to Nematic Transition in Solutions of Cylindrical PB–PEO Block Copolymer Micelles Close to a Wall

ARTICLE *in* LANGMUIR · SEPTEMBER 2003

Impact Factor: 4.46 · DOI: 10.1021/la034356a · Source: OAI

CITATIONS

13

READS

16

4 AUTHORS, INCLUDING:



Peter R Lang

Forschungszentrum Jülich

64 PUBLICATIONS 948 CITATIONS

SEE PROFILE



W. Pyckhout-Hintzen

Forschungszentrum Jülich

63 PUBLICATIONS 1,257 CITATIONS

SEE PROFILE

Isotropic to Nematic Transition in Solutions of Cylindrical PB–PEO Block Copolymer Micelles Close to a Wall

Peter Lang,^{*,†} Lutz Willner,[†] Wim Pyckhout-Hintzen,[†] and Rumen Krastev[‡]

Forschungszentrum Jülich, IFF, 52425 Jülich, Germany, and Hahn-Meitner-Institut, Glienicker-Strasse 100, 14109 Berlin, Germany

Received February 28, 2003. In Final Form: June 27, 2003

The influence of a flat interface on the isotropic to nematic (I/N) phase transition was investigated for aqueous solutions of cylindrical micelles of polybutadiene–poly(ethylene oxide) block copolymers using specular neutron reflectivity. While the I/N transition in the bulk occurs at the solute volume fraction $\phi_{N/I}$, we observed the formation of a condensed layer close to a silicon single-crystal interface at volume fractions of about $\phi_I \approx 0.85\phi_{N/I}$. The thickness of this layer does not vary if the solute fraction is changed, while its density increases drastically within a very narrow range of volume fractions. This observation is interpreted as the formation of a nematically ordered layer which is induced by the interface.

Introduction

In low molar mass systems, the effect of surface condensation and accompanying wetting phenomena has been investigated in great detail during the last two decades. For a variety of low molar mass single and multicomponent systems, it has been observed that order to disorder transitions are shifted by the presence of a flat interface, in such a way that the higher ordered phase is stable close to the interface, while in the bulk the system is in the less ordered state at the same thermodynamic conditions.^{1–7} However, the wetting behavior of the ordered phase depends very sensitively on the chemical structure and the molecular interaction of the respective compounds. A classical example of surface condensation with complete wetting is the formation of smectic films on top of nematic liquid crystals,^{2,8} while surface crystallization with incomplete wetting has been observed for higher *n*-alkanes.³

Similar to low molar mass mesogens, suspensions of colloidal rods also form liquid crystalline phases at higher volume fractions. The phase transition from the isotropic to the nematic phase (I/N) has been studied for many years. In his pioneering paper in 1949, Onsager formulated the first microscopic theory of the isotropic–nematic phase transition,⁹ and at present the phase behavior of a homogeneous system of hard rods is well understood. On the other hand, it is quite poorly understood how the presence of an interface influences the phase behavior of a suspension of rods. Only recently have a few theoretical

and simulation studies been devoted to this subject.^{10,11} In these studies, it is predicted that the interface between a hard wall and an isotropic fluid of hard rods induces two kinds of pretransitional ordering effects, that is, a uniaxial to biaxial transition at low volume fractions with subsequent wetting of the interface by the nematic phase. The nematic layer gives rise to a distinct concentration profile in which the rod concentration next to a wall is significantly higher than the concentration of the rods in the isotropic bulk. These studies are concerned with monodisperse rigid cylinder systems, which interact by a hard-body potential. An approach which takes into account a finite flexibility of the cylinders was published by Chen et al.;^{12,13} this approach also predicts the formation of a nematically ordered layer close to a wall, while the bulk material is still in the isotropic state. On the other hand, there are only very few systematic experimental reports on interface-induced ordering phenomena in colloidal suspensions.^{14,15} In particular, experiments on the isotropic to nematic pretransition of colloidal cylinder suspensions are completely absent. In this contribution, we present a first investigation of such a system, namely, aqueous solutions of the amphiphilic polybutadiene–poly(ethylene oxide) block copolymers (PB–PEO) against a silicon single-crystal interface.

There have been a large number of publications on the micellar morphologies and the structure of liquid crystalline mesophases formed in block copolymer solutions, and a corresponding large number of morphologies have been reported. In the field of water-based solutions, Förster et al. were the first to show that the morphology of polyelectrolyte micelles can be tuned by varying the respective block lengths and the ionic strength of the solvent.^{16,17} Besides polyelectrolyte-based copolymers, only very few types of block copolymers have been studied in aqueous

* To whom correspondence should be addressed. E-mail: p.lang@fz-juelich.de.

[†] Forschungszentrum Jülich.

[‡] Hahn-Meitner-Institut.

(1) Earnshaw, J. C.; Hughes, C. J. *Phys. Rev. A* **1992**, *46*, R4494.

(2) Als-Nielsen, J.; Christensen, F.; Pershan, P. S. *Phys. Rev. Lett.* **1992**, *48*, 1107.

(3) Ocko, B. M.; Wu, X. Z.; Sirota, E. B.; Sinha, S. K.; Gang, O.; Deutsch, M. *Phys. Rev. E* **1997**, *55*, 3164.

(4) Deutsch, M.; Wu, X. Z.; Sirota, E. B.; Sinha, S. K.; Ocko, B. M.; Magnussen, O. M. *Europhys. Lett.* **1995**, *30*, 283.

(5) Hayami, Y.; Findenegg, G. H. *Langmuir* **1997**, *13*, 4865.

(6) Gang, O.; Ellmann, J.; Möller, M.; Kraack, H.; Sirota, E. B.; Ocko, B. M.; Deutsch, M. *Europhys. Lett.* **2000**, *49*, 761.

(7) Marczuk, P.; Lang, P.; Findenegg, G. H.; Metha, S. K.; Möller, M. *Langmuir* **2002**, *18*, 6830.

(8) Lucht, R.; Marczuk, P.; Bahr, C.; Findenegg, G. H. *Phys. Rev. E* **2001**, *63*, 41704.

(9) Onsager, L. *Ann. N.Y. Acad. Sci.* **1949**, *51*, 627.

(10) van Roij, R.; Dijkstra, M.; Evans, R. *J. Chem. Phys.* **2000**, *113*, 7689.

(11) Dijkstra, M.; van Roij, R.; Evans, R. *Phys. Rev. E* **2001**, *63*, 1703.

(12) Cui, S. M.; Akcakir, O.; Chen, Z. Y. *Phys. Rev. E* **1995**, *51*, 4548.

(13) Chen, Z. Y.; Cui, S. M. *Phys. Rev. E* **1995**, *52*, 3876.

(14) Lang, P. *J. Phys. Chem. B* **1999**, *103*, 5100.

(15) Madsen, A.; Konovalov, O.; Robert, A.; Grübel, G. *Phys. Rev. E* **2001**, *64*, 061406.

(16) Förster, S.; Hermsdorf, N.; Leube, W.; Schnablegger, H.; Regenbrecht, M.; Akari, S.; Lindner, P.; Böttcher, C. *J. Phys. Chem. B* **1999**, *103*, 6657.

(17) Regenbrecht, M.; Akari, S.; Förster, S.; Möhwald, H. *J. Phys. Chem. B* **1999**, *103*, 6669.

solution. They may be divided into three groups, which are all based on PEO blocks as the hydrophilic part. Most of the contributions report on solutions of PEO–poly(propylene oxide)–PEO triblock copolymers, in which a wealth of different structures were observed.^{18,19} A second group is concerned with polymers that form aggregates that have glassy cores due to the high glass transition temperature of the hydrophobic moiety.^{20–23} In this case, desired morphologies can be tailored by elaborate processing. Finally, there are block copolymers with polyisoprene (PI–PEO),²⁴ poly(ethylene propylene) (PEP–PEO),^{25–28} and polybutadiene^{29–33} as the water-insoluble part, which all have low glass transition temperatures. In these cases, the micellar shape is determined by the length ratio of the blocks, the overall chain length of the polymer, and the solute concentration.

At small degrees of polymerization, PB–PEO block copolymers dissolve easily in water to form aggregates with spherical, cylindrical, or bilayer morphology. Only at large molar mass of the constituting unimers are more complex structures such as Y-junctions and networks observed.³³ For low molar mass copolymers with balanced block length, the formation of cylindrical micelles is favored. These micelles attain nematic order at a solute volume fraction of about 5–10% and hexagonal order at higher concentrations.^{29,30}

We have synthesized two short-chained PB–PEO block copolymers, h-PB1,4–h-PEO and d-PB1,4–d-PEO, by anionic polymerization with similar molar mass of the respective blocks and predominantly 1,4 microstructure in the polybutadiene. The micellar shape in aqueous solution was analyzed by static light scattering (SLS) and small-angle neutron scattering (SANS). For the analysis of SLS data, the scattered intensity at a given concentration c and scattering vector $Q = (4\pi n/\lambda_0) \sin(\Theta/2)$ are converted to the quantity $Kc/R(Q)$, where n is the refractive index of the solution, Θ is the scattering angle, λ_0 is the wavelength of the incident light in vacuum, c is the solute concentration in units of g/mL, and K is an optical contrast factor. If the scattered intensity may be factorized into a structure contribution $S(Q, c)$ and a particle contribution $P(Q)$, one can write

$$\frac{Kc}{R(Q)} = \frac{1}{M_w S(Q, c) P(Q)} \equiv \frac{1}{M_{app}(c) P(Q)} \quad (1)$$

where M_w is the particle molar mass and $M_{app}(c)$ is the

so-called apparent molar mass at a given concentration. Since $P(Q=0) = 1$, extrapolation of $Kc/R(Q)$ to zero scattering vector yields $M_{app}(c)$. For sufficiently dilute solutions, $S(Q, c)$ can be expressed as a second-order virial expansion in c and consequently $1/M_{app}(c)$ may be extrapolated linearly to zero concentration. According to Zimm,³⁴ this yields $1/M_w$ as the intercept and the slope is $2A_2$ with A_2 being the second osmotic virial coefficient.

Consequently $S(Q=0, c)$, M_w , and A_2 can be obtained from SLS experiments. These quantities can be used to obtain qualitative information on the shape of the scattering particles, if the variation of $1/S(Q=0, X)$, with $X = 2A_2 M_w c$ as the reduced concentration, is analyzed.³⁵

More quantitative information on the shape of micelles is available from SANS experiments, if experimental scattering data, collected from sufficiently dilute samples, can be analyzed by nonlinear least-squares fitting to an appropriate model function for the particle scattering factor, $P(Q)$. The micrographs of PB–PEO micelles published by Won et al.²⁹ strongly suggest that the micellar cylinders have a significant flexibility, which must be taken into account in the analysis of SANS data. In recent years, there have been two approaches to construct a particle scattering factor for semiflexible cylindrical particles,^{36,37} which both make use of the fact that the length scales of the micellar contour length, L_c , and the cross-section radius, R_{cs} , are well separated. In this case, $P(Q)$ may be factorized into a length contribution $P(Q, L_c, b, U)$ and a contribution of the cross section, $P(Q, R_{cs})$, where b is the statistical Kuhn segment length³⁸ and U is the length polydispersity index. While Pedersen et al. developed a semiempirical expression based on simulation results for $P(Q, L_c, b, U)$, Menge et al. used the expression given earlier by Koyama.³⁹ In this contribution, we used the method by Menge et al. for reasons which are discussed in their paper.

A very powerful tool to investigate the effect of the Si interface on the N/I transition is neutron reflectivity (NR).⁴⁰ In NR, one measures the specular reflectivity of neutrons as a function of the scattering vector $Q_z = (4\pi/\lambda) \sin \alpha$ normal to the surface, where α is the reflection angle. The reflectivity $R(Q_z)$ is related to the scattering length density profile in the direction normal to the surface, $\rho(z)$. A perfectly smooth interface between two half-spaces, each with constant $\rho(z)$ up to the interface, yields a monotonically decaying $R(Q_z)$ versus Q_z curve, while the presence of a layer with a different scattering length density adjacent to the interface causes an undulation of the reflectivity curve. The period of this undulation is related to the layer thickness, while its amplitude is related to the scattering length density of the layer. For the quantitative analysis of NR data, a model-independent method^{41,42} can be applied as well as the commonly used so-called multibox (or slab) model⁴³ in which the profiles

- (18) Alexandridis, P. *Curr. Opin. Colloid Interface Sci.* **1997**, *2*, 478.
 (19) Alexandridis, P.; Lindman, B. Eds. *Amphiphilic Block Copolymers: Self-Assembly and Application*; Elsevier: New York, 2000.
 (20) Cameron, N. S.; Corbierre, M.; Eisenberg, A. *Can. J. Chem.* **1999**, *77*, 1.
 (21) Zhang, L.; Eisenberg, A. *Science* **1995**, *268*, 1728.
 (22) Yu, K.; Zhang, L.; Eisenberg, A. *Langmuir* **1996**, *12*, 5980.
 (23) Burke, S.; Eisenberg, A. *High Perform. Polym.* **2000**, *12*, 535.
 (24) Deng, Y.; Young, R. N.; Rayn, A. J.; Fairclough, J. P. A.; Norman, A. I.; Tack, R. D. *Polymer* **2002**, *43*, 7155.
 (25) Willner, L.; Poppe, A.; Allgaier, J.; Monkenbusch, M.; Lindner, P.; Richter, D. *Europhys. Lett.* **2000**, *51*, 628.
 (26) Kaya, H. Ph.D. Thesis, Universität Münster, Münster, Germany, 2003.
 (27) Poppe, A.; Willner, L.; Allgaier, J.; Stellbrink, J.; Richter, D. *Macromolecules* **1997**, *30*, 7462.
 (28) Kaya, H.; Willner, L.; Allgaier, J.; Stellbrink, J.; Richter, D. *Appl. Phys. A* **2002**, *74*, 499.
 (29) Won, Y. Y.; Davis, H. T.; Bates, F. S. *Science* **1999**, *283*, 960.
 (30) Hentze, H. P.; Krämer, E.; Berton, B.; Förster, S.; Antonietti, M.; Dreja, M. *Macromolecules* **1999**, *32*, 5803.
 (31) Egger, H.; Nordskog, A.; Lang, P.; Brandt, A. *Macromol. Symp.* **2000**, *162*, 291.
 (32) Nordskog, A.; Egger, H.; Findenegg, G. H.; Schlaad, H.; von Berlepsch, H.; Böttcher, C. *Phys. Rev. E*, in press.
 (33) Jain, S.; Bates, F. S. *Science* **2003**, *300*, 460.

- (34) Zimm, B. H. *J. Chem. Phys.* **1948**, *16*, 1093.
 (35) Burchard W. In *Light Scattering: Principles and Development*; Brown, W., Ed.; Clarendon Press: Oxford, 1996.
 (36) Pedersen, J. S.; Schurtenberger, P. *Macromolecules* **1996**, *29*, 7602.
 (37) Menge, U.; Lang, P.; Findenegg, G. H.; Strunz, P. *J. Phys. Chem. B* **2003**, *107*, 1316.
 (38) Kuhn, W. *Kolloid Z.* **1934**, *68*, 2.
 (39) Koyama, R. *J. Phys. Soc. Jpn.* **1973**, *34*, 1029.
 (40) Thomas, R. K. In *Modern Characterization Methods of Surfactant Systems*; Binks, B. P., Ed.; Surfactant Science Series 83; Marcel Dekker: New York, 1999.
 (41) Zhou, X. L.; Chen, S. H. *Phys. Rev. E* **1993**, *47*, 3174.
 (42) Pedersen, J. S. *J. Appl. Crystallogr.* **1992**, *25*, 129.
 (43) Als-Nielsen, J.; Jacquemain, D.; Kjaer, K.; Leveiller, F.; Lahav, M.; Leiserowitz, L. *Phys. Rep.* **1994**, *246*, 251.

are analyzed in terms of box height, box density, and the roughness parameter of the interface between adjacent boxes.

The paper is organized as follows. First we present the bulk scattering experiments on PB-PEO in aqueous solution and their analysis. In the main part of the paper, we report NR data from the interface between a Si single crystal and solutions of PB-PEO with different scattering contrasts. The data are analyzed in terms of the thickness and density of a condensed layer close to the interface. In the discussion, we compare our experimental observations to theoretical predictions for hard-rod fluids and solutions of semiflexible liquid crystalline polymers.

Experimental Section

Synthesis of the block copolymers h-PB1,4-h-PEO and d-PB1,4-d-PEO was accomplished by anionic polymerization. The polymerization was realized by a two-step process, because each block requires different reaction conditions. At first, two polybutadienes with a high degree of 1,4-microstructure were synthesized from 1,3-butadiene- d_6 (Chemotrade, Leipzig, Germany, 98% d) and 1,3-butadiene- h_6 , respectively, using *tert*-butyllithium as the initiator and benzene as the reaction solvent. The living polymers were end capped by the addition of an excess amount of either ethylene oxide- d_4 (CDN Isotopes, Quebec, Canada, 99.8% d) or ethylene oxide- h_4 and were terminated with acetic acid. Since no propagation of EO takes place with lithium as a counterion in nonpolar media, the chain end is functionalized by exclusively one hydroxyethyl group. The two polymers, h-PB1,4-OH and d-PB1,4-OH, were precipitated in methanol and dried in high vacuum until any kind of volatile impurity was removed. In the second polymerization step, naphthalene potassium was used to convert the PB-OH polymers into the macroinitiators h-PB1,4-OK and d-PB1,4-OK. These were used to polymerize EO- h_4 and EO- d_4 in THF at 50 °C for 2 days. The living polymers were terminated with acetic acid and then precipitated twice in acetone at -20 °C. A more detailed description of the synthetic procedure is given elsewhere.⁴⁴

The PB1,4-OH precursor polymers were characterized by size exclusion chromatography (SEC) at 30 °C using a Waters 150-CVplus chromatograph combined with a Viscotek model 300 triple detector array. Four ultra-styrigel columns covering a nominal porosity range from 100 to 10⁴ Å were used with tetrahydrofuran (THF) as the eluant at a flux rate of 1 mL/min. The system was conventionally calibrated using polystyrene standards with narrow molar mass distribution, and in addition, a set of well-defined polydiene standards were taken to generate a universal calibration curve. Polydispersities, M_w/M_n , were calculated from the conventional calibration curve, while molar masses were extracted from universal calibration. The absolute molar mass of the fully proteated polymer, h-PB1,4-OH, was determined by ¹H NMR spectroscopy using a Bruker AMX 300 instrument. The number-average molar mass, M_n , was calculated by comparison of the signal intensities arising from the PB repeat units with those from the nine protons of the initiator group. From the ¹H NMR spectrum, the microstructure of the polymer was determined to consist of 88% 1,4- and 12% 1,2- repeat units. For the deuterated polymer, the same microstructure was assumed since the polymer was prepared under analogous conditions.

The block copolymers were examined by SEC at 30 °C using a second chromatography setup consisting of a Waters 150C instrument and four ultra-Styrigel columns of constant pore size together with one column of continuous pore size covering an overall porosity range from 500 to 10⁵ Å. The run conditions were 1 mL/min flow of a mixture of THF and *N,N*-dimethylacetamide (90:10 by volume). Polystyrene standards with narrow molar mass distribution were used for calibration. The elution peaks of both block copolymers reveal narrow molar mass distributions without any sign of homopolymer contamination. The absolute molar mass of the h-PEO block in h-PB1,4-h-PEO was determined by ¹H NMR. Based on the known molar mass

Table 1. Molecular Characteristics of the Block Copolymers

block copolymer	PB		PEO	
	M_n (g/mol)	M_w/M_n^a	M_n (g/mol)	M_w/M_n^a
h-PB1,4-h-PEO	1600 ^b ; (1700 ^c)	1.06	1600 ^c	1.05
d-PB1,4-d-PEO	1750 ^b	1.06	1900 ^d	1.03

^a By conventional SEC. ^b By SEC with universal calibration. ^c By ¹H NMR. ^d Estimated from the comparison of the elution volumes of precursor and block copolymer.

of the h-PB1,4-OH block, M_n was determined by relating the signal intensities of PB with the intensity of PEO methylene units. The molar mass of the d-PEO in the fully deuterated block copolymer was estimated on the basis of the known d-PB1,4-OH molar mass and comparison of the elution volumes of proteated and deuterated precursor and block copolymers. A summary of the molecular characteristics of the polymers is given in Table 1.

Static light scattering experiments were performed on a series of h-PB1,4-h-PEO solutions in H₂O, which were prepared by dilution of a stock solution with a solute content of $c = 5.25 \times 10^{-3}$ g/mL. We used a commercial LS apparatus by ALV-Laservertriebsgesellschaft, Langen, Germany, which is equipped with a He/Ne laser with a power output of 15 mW and a wavelength of $\lambda_0 = 632$ nm as the primary light source. The scattering angle was varied from 20° to 150° in 5° steps to cover a range of scattering vectors $4.59 \times 10^{-4} \text{ Å}^{-1} \leq Q \leq 2.55 \times 10^{-3} \text{ Å}^{-1}$ depending slightly on the concentration as the refractive index of the solution is $n = n_0 + c \, dn/dc$. Here n_0 is the index of refraction of the pure solvent and dn/dc is the refractive index increment which was measured with the DR1 instrument from ALV. Reduced integrated excess intensities $R(Q)$ were derived from the relative scattered intensities $r(Q) = i(Q)/I_0$ and converted to the quantity $KcR(Q)$, where the contrast factor K was calculated according to the standard procedure, which is described in detail elsewhere.⁴⁵ Values of $1/S(Q=0)$ were determined by linear least-squares fitting of plots of $KcR(Q)$ versus Q^2 . Since $KcR(Q)$ did not depend linearly on Q^2 in the whole experimental range, we used only the initial part of the curves for the fitting where a correlation coefficient better than 0.99 could be obtained. This was typically the range below $\Theta \leq 50^\circ$ corresponding to $Q^2 \leq 1.25 \times 10^{-6} \text{ Å}^{-2}$.

Small-angle neutron scattering data were collected on the KWS1 instrument at the FRJ2 reactor (20 MW), Forschungszentrum Jülich GmbH (FZJ). Neutrons were derived from a hydrogen cold source and monochromatized by a velocity selector. The mean de Broglie wavelength was set to $\lambda_0 = 7$ Å with a full width spread of $\Delta\lambda/\lambda_0 = 0.2$. The instrument was equipped with a 64 × 64 Li-scintillation detector with a pixel size of 8 × 8 mm², which was positioned at three different sample-to-detector distances (2, 8, and 20 m) to cover a range of scattering vectors $2 \times 10^{-3} \text{ Å}^{-1} \leq Q \leq 0.15 \text{ Å}^{-1}$ after radial averaging. Solutions with a polymer concentration of 1 mg/mL were measured in quartz cells with a path length of 1 mm. Sampling times were chosen such that the statistical error was smaller than 2% at any scattering vector. Data reduction and calibration of intensities using Lupolene as a secondary standard were achieved by FCJ standard procedures.⁴⁶

Neutron reflectivity experiments were run at the reflectometer V6 of BENSC at the Hahn-Meitner Institute, Berlin, Germany. A detailed description of the instrument is given elsewhere.⁴⁷ The neutron de Broglie wavelength was set to 4.66 Å by an array of single-crystal graphite monochromators in the white beam. The incoming beam cross-section profile was defined by two adjustable slits inserted between the monochromators and the sample. The scattered neutrons were recorded with a ³He detector. The primary intensity was monitored with a counter placed directly in the incident beam path.

(45) Menge, U.; Lang, P.; Findenegg, G. H. *J. Phys. Chem. B* **1999**, 103, 5768.

(46) Pyckhout-Hintzen, W.; Springer, T.; Forster, F.; Gronski, W.; Fischkorn, C. *Macromolecules* **1991**, 24, 1269.

(47) Mezei, F.; Goloub, R.; Klose, F.; Toews, H. *Physica B* **1995**, 213/214, 898.

(44) Allgaier, J.; Poppe, A.; Willner, L.; Richter, D. *Macromolecules* **1997**, 30, 1582.

Reflectivity scans were conducted on two dilution series, the first consisting of the proteated diblock copolymer dissolved in D₂O and the second of the deuterated diblock copolymer dispersed in a D₂O/H₂O mixture. The composition of the isotopic water mixture was adjusted to match the scattering length density of single-crystalline silicon (so-called null reflecting water). As sample cells, we used Vespel troughs with a volume of $2.5 \times 75 \times 45 \text{ mm}^3$ which were covered with Si single crystals with a size of $25 \times 50 \times 80 \text{ mm}^3$. Since single-crystalline silicon is transparent for neutrons, the reflectivity measurement from the solid/liquid interface could be performed in an $\alpha/2\alpha$ geometry where α is the sample angle and 2α is the detector angle with respect to the incident beam direction. Each reflectivity scan covered a range of scattering vectors from $Q_z = 4.7 \times 10^{-3}$ to 0.155 \AA^{-1} for the solutions of proteated diblock copolymer in D₂O. In the case of solutions of deuterated diblock copolymer in null reflecting water, the incoherent background scattering was much higher, thus reducing the highest scattering vector at which a reasonable signal-to-noise ratio was observed to $Q_z \leq 0.0518 \text{ \AA}^{-1}$. The incident beam was collimated by the slit system to a rectangular cross section of $0.5 \times 40 \text{ mm}^2$ if $Q_z \leq 0.0518 \text{ \AA}^{-1}$ and of $1.0 \times 40 \text{ mm}^2$ elsewhere. Accordingly the resolution was $\Delta Q_z \approx 10^{-3} \text{ \AA}^{-1}$ in the low Q_z -range and $\Delta Q_z \approx 2 \times 10^{-3} \text{ \AA}^{-1}$ in the range above $Q_z = 0.0518 \text{ \AA}^{-1}$. The background noise was collected simultaneously to the specularly reflected signal with a ³He counter offset from the specular position by 0.44° toward larger scattering angles. It was directly subtracted from the specular signal to obtain the background-corrected intensity. At small angles, the samples were overilluminated and therefore the reflectivity data were footprint corrected for the varying flux on the sample as α increased and normalized to the measured incident intensity to obtain the reflectivity $R(Q_z)$.

The solutions were filled into the cells through access holes in the bottom of the troughs which could be closed with nylon screws. Since the solutions were flow-birefringent, prior to the measurement they were allowed to relax for at least 3 h and up to 30 h in the case of the solutions with the highest polymer volume fractions. For this reason, it was not possible to record reflectivity data for proteated polymers in D₂O with volume fractions higher than $\phi = 0.067$. For the deuterated diblock copolymer in null reflecting water, the accessible range of volume fractions was $\phi \leq 0.059$.

Results and Discussion

Binary mixtures of h-PB1,4-h-PEO in D₂O and of d-PB1,4-d-PEO in null reflecting water are permanently birefringent at volume fractions at which the solutions are in the nematic state. The location of the isotropic to nematic phase transition in the bulk was determined by visual inspection of the solutions between crossed polarizers. In neither case could we observe a complete macroscopic separation of the coexisting phases, but the solutions of the proteated sample in H₂O were completely isotropic at volume fractions $\phi \leq 0.078$ and the solutions with the deuterated polymer in null reflecting water showed birefringent speckles above $\phi > 0.06$.

The different phase behavior hints at a significant difference in the morphology of the micelles, which form the nematic phase. This is actually expected as the PEO-block length of the deuterated sample is larger than that of the proteated polymer. The micellar morphology depends very subtly on the ratio of the respective block length.^{25,26,30} It is thus essential to determine the micellar shape for the two polymers, prior to the investigation of the phase behavior close to an interface. To this end, we performed static light scattering and small-angle neutron scattering experiments.

For solutions of the proteated polymer in H₂O with concentrations up to $c = 5.25 \times 10^{-3} \text{ g/mL}$, we determined the zero scattering vector structure factor $S(Q=0)$ by linear least-squares fitting of $1/M_{\text{app}}$ versus c . From the low-concentration data at $c \leq 2 \times 10^{-4} \text{ g/mL}$, we extracted the mass-average molar mass $M_w = (1.6 \pm 0.1) \times 10^8 \text{ g/mol}$

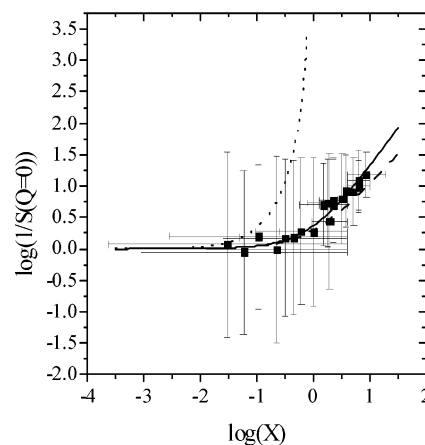


Figure 1. Inverse zero angle structure factor $S(Q=0)^{-1}$ versus reduced concentration $X = 2A_2M_w c$. The symbols are experimental data from solutions of proteated h-PB1,4-h-PEO in H₂O, and the lines are theoretical predictions for solutions of hard spheres (dotted), semiflexible polymer chains (full), and hard rods (dashed). The error bars represent the uncertainties resulting from the linear least-squares fitting of the SLS data.

of the micelles and the second osmotic virial coefficient $A_2 = (8 \pm 1) \times 10^{-6} \text{ mL g}^{-1} \text{ mol}^{-1}$.

In Figure 1, $S(Q=0)^{-1}$ is plotted versus the reduced concentration $X = 2A_2M_w c$ on a double logarithmic scale. The errors represent the uncertainty of the linear least-squares fitting of $1/M_{\text{app}}$ versus c . In this representation, $S(Q=0)^{-1}$ is sensitive to the particle shape,³⁵ as is visualized by the theoretical curves for hard spheres,^{48,49} semiflexible polymer chains,⁵⁰ and hard rods,⁹ which are displayed for comparison. Despite the large experimental uncertainties, it is obvious from Figure 1 that the micelles are nonspherical. However, it is not possible to distinguish from these data whether the micelles behave like hard rods or as semiflexible cylinders, nor is any information about the micelles' cross-sectional dimensions available from SLS.

Therefore, we performed SANS experiments at a concentration of 1 mg/mL at which the structure factor of the solution $S(Q)$ is only insignificantly different from unity according to the light scattering experiments. In Figure 2, the radially averaged scattered intensities corrected for solvent and background scattering are plotted versus the scattering vector Q .

We attempted to fit the experimental data with the model function for rigid cylinders with a Gaussian distribution of cross-section radii, as was suggested by Won et al.²⁹ for micelles of PB1,2-PEO block copolymers which had block lengths and PB microstructure different from the block copolymers used in this study. However, we were not able to get satisfactory results with this approach; especially the low- q part of the scattering curves could not be fitted, while the high- q part which is due to the cross-section scattering was reproduced reasonably well. A closer look at the micrographs presented in the contribution by Won et al.²⁹ reveals that the micelles exhibit a remarkable flexibility. Therefore we used a model function for semiflexible cylinders to fit the SANS data, which we had developed recently³⁷ along the ideas of Pedersen et al.³⁶ If the length scale of the cylinder contour length, L_c , and its cross-section radius, R_{cs} , are sufficiently separated, the finite cross-section diameter of the cylinders can be taken into account by multiplying Koyama's

(48) Percus, J. K.; Yevick, G. J. *Phys. Rev.* **1958**, *110*, 1.

(49) Carnahan, N. F.; Starling, K. E. *J. Chem. Phys.* **1969**, *51*, 635.

(50) Ohta, T.; Oono, Y. *Phys. Lett.* **1982**, *89A*, 460.

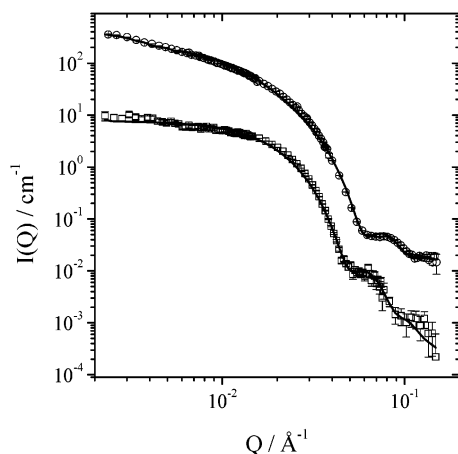


Figure 2. SANS curves from aqueous solutions of PB-PEO block copolymers with a concentration of $c = 1$ mg/mL. The open circles are data from the proteated diblock in D_2O , while the open squares are data from the deuterated polymer in null reflecting water. The latter are displaced on the ordinate by a factor of 0.1 for clarity. The full lines are best fits of the model described in the text.

expression for the particle scattering factor of a polydisperse wormlike chain,³⁹ $P_{wlc}(Q, L_c, b, U)$, with the cross-section form factor of a rigid homogeneous cylinder $P_{cs}(Q, R_{cs})$, that is,

$$P(Q, L_c, b, U, R_{cs}) = P_{wlc}(Q, L_c, b, U) P_{cs}(Q, R_{cs}) \quad (2)$$

where b is the statistical Kuhn segment length, U is the polydispersity index of the contour length, and

$$P_{cs}(Q, R_{cs}) = \left[\frac{2J_1(QR_{cs})}{QR_{cs}} \right]^2 \quad (3)$$

where R_{cs} is the cross-section radius and $J_1(QR_{cs})$ is the first-order Bessel function. In the fitting algorithm, the model function of eq 2 was multiplied by an amplitude $I(Q=0)$ and data-smearing with a Gaussian-type resolution function as suggested by Pedersen⁵¹ was taken into account. Although we took into account experimental data-smearing, the minima in the scattering curves could not be reproduced properly by this model. Especially in the case of the deuterated polymer in nonreflecting water, the minima were much too sharp and too deep. As already discussed above, this part of the curves could be well fitted with a model which accounts for polydispersity of the cross-section diameter. Consequently, we further modified our model function, taking into account a Gaussian distribution of cross-section radii. This procedure is rather time-consuming, since $P_{wlc}(Q, L_c, b, U)$ contains two integrations, which can only be solved numerically,^{39,52} and two further numerical integrations are required, one to account for the distribution of the cross section and another for experimental smearing. To reduce computer time, the polydispersity index was fixed to $U = 2$. The full lines in Figure 2 are the best fits of this model to the experimental data, and the resulting parameter values are summarized in Table 2.

We note that the overall micellar contour length, L_c , of the deuterated polymer is significantly smaller than in the case of the proteated polymer while R_{cs} is larger for the deuterated micelles due to the higher degree of polymerization of the unimer PEO block (see Table 1).

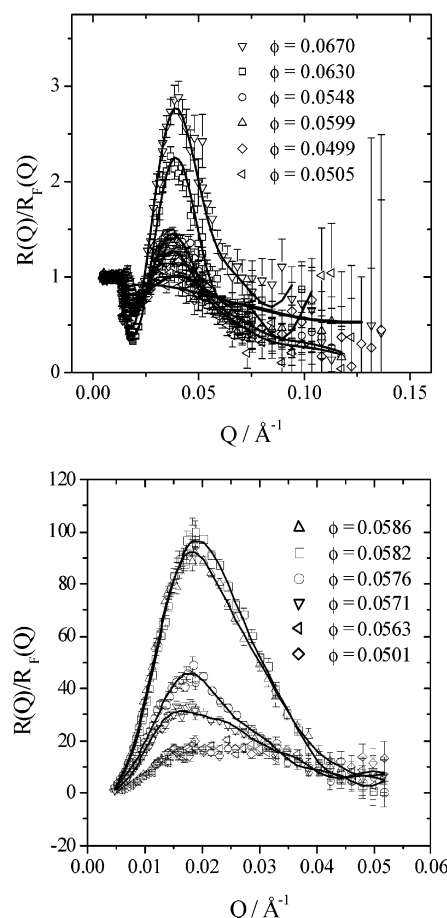


Figure 3. Normalized reflectivity data from an interface between a Si single crystal and solutions of h-PB1,4-h-PEO in D_2O (top) and d-PB1,4-d-PEO in null reflecting water (bottom), respectively. The volume fractions of the solutions are indicated in the legends.

Table 2. Mean Contour Length, L_c , Kuhn Segment Length, b , and Mean Cross-Section Radius, R_{cs} , and Its Variance $\sigma_{R_{cs}}$ of the Block Copolymer Micelles Determined by Nonlinear Least-Squares Fitting of the Model Function to SANS Data as Described in the Text

block copolymer	L_c (Å)	b (Å)	R_{cs} (Å)	$\sigma_{R_{cs}}$
h-PB1,4-h-PEO	3800 ± 100	59 ± 15	67 ± 2	0.15
d-PB1,4-d-PEO	590 ± 70	70 ± 15	83 ± 2	0.09

Consequently the aspect ratio is smaller in the case of the deuterated micelle, which corresponds to a higher mean curvature of the hypothetical plane that separates the hydrophobic core from the aqueous surroundings. This is well in line with other experimental findings^{25,26,30} and the concept of spontaneous curvature of amphiphilic films.⁵³

To study the influence of a hard wall on the N/I phase transition, we performed neutron reflectivity scans from the interface between a silicon single crystal and solutions of PB1,4-PEO block copolymers at two different scattering contrasts. The normalized reflectivity curves of a series of solutions containing proteated polymer dispersed in D_2O are plotted in the top of Figure 3a as $R(Q_z)/R_F(Q_z)$ versus Q_z where $R_F(Q_z)$ is the theoretical Fresnel reflectivity from a perfectly flat interface between the silicon and a fictitious solution with the same scattering length density, ρ , as the mean bulk value of the investigated

(51) Pedersen, J. S. *J. Appl. Crystallogr.* **1990**, *23*, 321.

(52) Schmidt, M. *Macromolecules* **1984**, *17*, 553.

(53) See for example: Israelachvili, J. N. *Intermolecular and Surface Forces*; Academic Press: London, 1985.

solution. In this representation, the reflectivity from a perfectly smooth interface between two half-spaces would yield unity throughout the whole range of scattering vectors, if the scattering length densities of both half-spaces were constant up to the interface ($z = 0$). In a real experiment, the curve would slightly decay with increasing Q_z as the reflectivity is damped by the intrinsic roughness of the interface. However, if there is a thin layer at the interface which has a scattering length density different from the bulk value, the normalized reflectivity curve shows undulations. The periodicity of the undulations is inversely proportional to the thickness of the layer, and their amplitude is proportional to the scattering length density of the layer. All experimental curves in Figure 3a show a maximum region where $R(Q_z)/R_F(Q_z) > 1$, which is very shallow at volume fractions $\phi < 0.06$. Above this volume fraction, the maximum value increases by a factor of about 3 in a very narrow regime while the position of the maximum does not change. The same features, although more pronounced, can be seen in Figure 3b where the data from solutions of deuterated polymer in null reflecting water are shown. Here the $R(Q_z)/R_F(Q_z)$ curves for the two lowest volume fractions are indistinguishable with a maximum value of ca. 20. Then the maximum value increases up to roughly 100 in the very narrow range of $0.0563 < \phi < 0.0582$, while the position of the maximum remains unchanged. Upon further increase of the volume fraction, the maximum value remains constant as well. This shows unambiguously that a layer is formed close to the interface at volume fractions $\phi > 0.057$ in the case of the deuterated polymer in null reflecting water and above $\phi > 0.06$ for the proteated polymer in D_2O . In both cases, the scattering length density of this layer is different from the bulk value of the solution, ρ_{bulk} , and it varies strongly with the bulk volume fraction, while the average thickness of the layer is invariant. These observations are strong evidence for the formation of an interfacial region which is nematically preordered, since the number density of the polymer is higher in the nematic phase than in the isotropic solution.

To get a more quantitative picture of this interfacial layer, we determined the scattering length density profiles from the reflectivity curves. This is an inverse problem, for which various solution strategies have been proposed.⁵⁴ Here we applied a two-step strategy. First we used a model-independent method (GTM-SA)⁷ which combines the so-called groove tracking method⁴¹ with the simulated annealing technique.⁵⁵ The profiles obtained by GTM-SA were used to estimate reasonable starting values for the fitting of a multibox (or slab) model⁴³ to the experimental data.

The results are displayed graphically in Figure 4. In the case of deuterated polymers in null reflecting water, we were not able to get any reasonable fits at polymer volume fractions $\phi < 0.0571$, due to the low signal-to-noise ratio of the experimental data. For the same reason, we could not get reasonable reflectivity data at $q_{\text{max}} > 0.05 \text{ \AA}^{-1}$ from the deuterated polymer in null reflecting water (see also Experimental Section). This limits the spatial resolution of the experiment to distances larger than $\Delta d_{\text{min}} = 2\pi/q_{\text{max}} \approx 125 \text{ \AA}$. We will therefore not discuss the profiles displayed in Figure 4 in detail, except for the observations that the thickness of the region where the scattering length density deviates from the bulk value, d , is in the order of a few micellar segment lengths, b , as

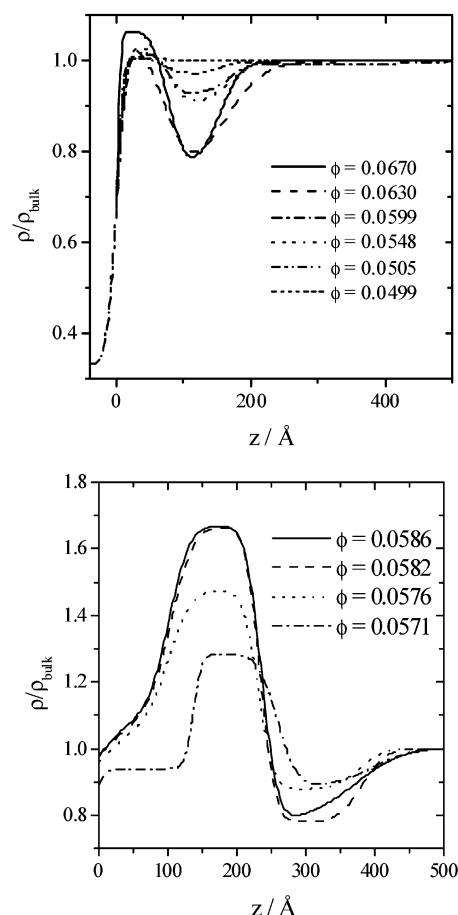


Figure 4. Normalized scattering length density profiles of an interface between a Si single crystal and solutions of h-PB1,4-h-PEO in D_2O (top) and d-PB1,4-d-PEO in null reflecting water (bottom), respectively. The volume fractions of the solutions are indicated in the legends.

determined by SANS and not in the order of the contour length L_c . Further, we note that d is independent of the bulk volume fraction within the resolution of the experiment.

This observation is in contradiction to the theoretical predictions for the interface-induced I/N pretransition of a hard-rod system.^{10,11} There it is expected that hard rods form a nematically preordered phase next to a wall at $\phi_i \approx 0.85\phi_{IN}$. However, the thickness of this layer should initially be of the order of the rod length. In light of the high flexibility of the micelles, this discrepancy is not surprising. One would rather expect the micelles to behave like semiflexible main chain liquid crystalline polymers. In this model, the mesogenic entities can be identified with the Kuhn segments of the chain.

With the approximation that the Kuhn segments may be treated as Onsager rods ($b \gg R_{cs}$), Chen et al.^{12,13} calculated the segment density profile perpendicular to a wall using a density functional theory. Like the theory for hard rods, this theory also predicts an interfacial pretransition at roughly $\phi_i \approx 0.8\phi_{IN}$. However, the thickness of the preordered layer is expected to be initially of the order of the Kuhn length, b , and a significant increase of the thickness is only expected for $\phi > 0.99\phi_{IN}$. Accordingly, our experimental observation that the thickness of the nematic layer is of the order of a few segment lengths may be regarded as qualitative agreement with the prediction by Chen et al. The fact that we did not observe the predicted divergence of the layer thickness is due to technical reasons. Solutions with $\phi > 0.9\phi_{IN}$ show

(54) For an overview see: Lovell, R. M.; Richardson, R. M. *Curr. Opin. Colloid Interface Sci.* **1999**, *4*, 197.

(55) Kirkpatrick, S.; Gelatt, C. O.; Vecchi, M. P. *Science* **1983**, *220*, 671.

strong flow birefringence, which, if not relaxed, might mimic nematic ordering in the experiments. Since the relaxation times exceeded 30 h, it was not practical to collect more reflectivity data in this range of polymer volume fractions. We can therefore not distinguish whether the nematic layer wets the interface or not. In any case, the agreement with the theoretical prediction has to remain on a qualitative level because the segments of our block copolymer micelles have a finite aspect ratio, while the theory assumes that $b \gg R_{cs}$.

Conclusions

By anionic polymerization, we have synthesized amphiphilic block copolymers, which form cylindrical micelles in aqueous solutions. The structural parameters of these micelles were determined by SANS. Despite the high flexibility of the micelles, their solutions form a nematic phase at sufficiently high polymer volume fractions. The influence of a hard wall on the formation of the nematic phase was studied by neutron reflectivity. From the reflectivity data, it can be seen without any detailed analysis that the isotropic to nematic transition is shifted to lower volume fractions in a layer close to the wall. The thickness of this layer does not depend on the bulk volume fraction of the polymer, ϕ , while its density increases

drastically with increasing ϕ . The quantitative analysis of the reflectivity data in terms of scattering length density profiles confirms these observations. Further, the thickness of the nematic layer is found to be of the order of a few Kuhn segment lengths of the micelles. In particular, this last finding shows that the behavior of the block copolymer micelles close to a wall cannot be described by the theory for hard rods.^{10,11} We rather find that our experimental observations are in qualitative accord with the predictions by Chen et al.^{12,13} for a nematic pretransition close to a wall for semiflexible polymers. Since this theory is based on the assumption that the segments can be treated as Onsager rods, a quantitative agreement with the experiment cannot be expected. To remove this deficiency, we are currently setting up a simulation scheme which takes into account the finite aspect ratio of the segments.

Acknowledgment. The authors thank Gerd Meier for his help with the SANS experiments, Johan Buitenhuis and Zvonimir Dogic for their assistance with the reflectivity measurements, Jörg Stellbrink for giving access to the light scattering apparatus, and the Berlin Neutron Scattering Center (BENSCH) for the reflectivity beam time.

LA034356A